Generating carbon schwarzites via zeolite-templating

Efrem Braun[a], Yongjin Lee[b,c], Seyed Mohamad Moosavi[b], Senja Barthel[b], Rocio Mercado[d], Igor A. Baburin[e], Davide M. Proserpio[f,g], and Berend Smit[a,b,1]

[a]Department of Chemical and Biomolecular Engineering, University of California, Berkeley, CA 94720; [b]Institut des Sciences et Ingénierie Chimiques (ISIC), Valais, École Polytechnique Fédérale de Lausanne (EPFL), CH-1951 Sion, Switzerland; [c]School of Physical Science and Technology, ShanghaiTech University, Shanghai 201210, China; [d]Department of Chemistry, University of California, Berkeley, CA 94720; [e]Theoretische Chemie, Technische Universität Dresden, 01062 Dresden, Germany; [f]Dipartimento di Chimica, Università degli Studi di Milano, 20133 Milan, Italy; and [g]Samara Center for Theoretical Materials Science (SCTMS), Samara State Technical University, Samara 443100, Russia

Edited by Monica Olvera de la Cruz, Northwestern University, Evanston, IL, and approved July 9, 2018 (received for review March 25, 2018)

Zeolite-templated carbons (ZTCs) comprise a relatively recent material class synthesized via the chemical vapor deposition of a carbon-containing precursor on a zeolite template, followed by the removal of the template. We have developed a theoretical framework to generate a ZTC model from any given zeolite structure, which we show can successfully predict the structure of known ZTCs. We use our method to generate a library of ZTCs from all known zeolites, to establish criteria for which zeolites can produce experimentally accessible ZTCs, and to identify over 10 ZTCs that have never before been synthesized. We show that ZTCs partition space into two disjoint labyrinths that can be described by a pair of interpenetrating nets. Since such a pair of nets also describes a triply periodic minimal surface (TPMS), our results establish the relationship between ZTCs and schwarzites—carbon materials with negative Gaussian curvature that resemble TPMSs—linking the research topics and demonstrating that schwarzites should no longer be thought of as purely hypothetical materials.

schwarzite | zeolite-templated carbon | triply periodic minimal surface | template carbonization | microporous carbon

The search for new forms of carbon has not stopped with the discovery of fullerenes and graphene. Indeed, there are over 500 unique triply periodic hypothetical carbon structures present in the Samara Carbon Allotrope Database, with the vast majority having been proposed in the last decade (1). Many of these hypothetical carbon allotropes take the form of schwarzites, which are carbon structures that mimic a triply periodic minimal surface (TPMS) (1–6). The interest in synthesizing these novel materials is motivated not only by the scientific beauty of these surfaces but also by the predictions that they have unique electronic, magnetic, and optical properties that may make them useful for applications such as supercapacitors, battery electrodes, catalysis, gas storage, and separations (7–11).

The synthesis of these materials has been challenging (10, 12). Amorphous carbons consisting of local regions with negative Gaussian curvature have been observed [e.g., Bourgeois and Bursill (13) and Barborini et al. (14)]. These materials have been noted to be similar to "random schwarzite" models that have local properties similar to schwarzites (15), but they lack the long-range ordering required for characterization of their topologies by the periodic nets that describe TPMSs (16–18).

A true breakthrough has been the development of the template carbonization process, in which a carbon-containing precursor is introduced into a porous structured template and carbonized, followed by removal of the template (19–23). Varying the template structure can bring about a wide variety of carbon materials, including one-dimensional nanotubes and nanorods, 2D graphene stacks, and 3D ordered mesoporous or microporous carbons (21, 23).

Of interest for this work is when a zeolite is used as a template, with the resulting liberated carbon material referred to as a zeolite-templated carbon (ZTC) (21, 22). A motivation of this work is the discussion in the literature about whether a ZTC can be seen as a schwarzite (24–28). Indeed, the experimental properties of ZTCs are exactly those which have been predicted for schwarzites, and hence ZTCs are considered as promising materials for the same applications (21, 22). As we will show, the similarity between ZTCs and schwarzites is striking, and we explore this similarity to establish that the theory of schwarzites/TPMSs is a useful concept to understand ZTCs. In particular, we will focus on the role of the template in determining whether a stable ZTC will form. At present, the selection of zeolite templates for this process has been based on trial and error, and in this work, we provide a rationale for why the three commonly used zeolite templates—FAU, EMT, and beta [when possible, we use the International Zeolite Association (IZA) three-letter code to represent a particular zeolite structure (29)]—have been successful (22, 30, 31). In addition, our approach yields suggestions for over 10 additional zeolite structures that can be used for ZTCs that have not yet been synthesized.

In Silico Generation of ZTC Structures

Unlike zeolites, ZTCs are not crystalline; instead, they are nonperiodic orderings of atoms on periodic surfaces. Consequently, we cannot simply take the crystal structure as a starting point

Significance

Nanocarbons can be characterized by their curvature—that is, positively curved fullerenes, zero-curved graphene, and negatively curved schwarzites. Schwartzites are fascinating materials but have not been synthesized yet, although disordered materials with local properties similar to schwarzites ("random schwarzites") have been isolated. A promising synthetic method allows for the interior surfaces of zeolites to be templated with sp^2 carbon, but theoretical study of these zeolite-templated carbons (ZTCs) has been limited because of their noncrystalline structures. In this work, we develop an improved molecular description of ZTCs, show that they are equivalent to schwartzites, and thus make the experimental discovery of schwarzites ex post facto. Our topological characterization of ZTCs lends insights into how template choice allows for the tunability of ordered microporous carbons.

Author contributions: E.B. and B.S. designed research; E.B., Y.L., S.M.M., S.B., R.M., I.A.B., and D.M.P. performed research; and E.B., S.M.M., S.B., D.M.P., and B.S. wrote the paper.

Conflict of interest statement: The authors, the University of California, and EPFL have filed a provisional patent application on some of the results contained herein.

This article is a PNAS Direct Submission.

Data deposition: All files containing atomic coordinates are available for download from the Open Science Framework at doi.org/10.17605/OSF.IO/ZHDB2 and from the Materials Cloud at doi.org/10.24435/materialscloud:2018.0013/v1.

[1]To whom correspondence should be addressed. Email: berend.smit@epfl.ch.

This article contains supporting information online at www.pnas.org/lookup/suppl/doi:10.1073/pnas.1805062115/-/DCSupplemental.

Published online August 14, 2018.

for a molecular simulation. The in silico generation of a sufficiently reliable ZTC structure for a given zeolite template is therefore an essential first step, for which two methods have so far been proposed. Nishihara and coworkers assembled carbon atoms inside the pores of FAU to match the ZTC-FAU carbon loading determined experimentally (26, 28, 32). Roussel et al. instead used a grand-canonical Monte Carlo (GCMC) scheme that results in a ZTC model with a carbon loading dependent on the choice of chemical potential (24, 25, 33); they subsequently tuned the chemical potential such that a structure was obtained with carbon neither undertemplating the zeolite surface nor filling in the zeolite's void space.

To avoid some of the limitations of the existing methods, we developed a Monte Carlo (MC) algorithm that aims to fully template the zeolite surface, providing a well-defined upper limit of the experimentally achievable carbon loading (see *SI Appendix* for a discussion on carbon loadings). Our method closely mimics the synthetic process, in which the carbon precursor catalytically decomposes upon contact with the zeolite surface, forming a new surface of sp^2-hybridized carbon atoms (22, 27, 31). Accordingly, our algorithm inserts sp^2-hybridized carbon atoms next to unsaturated carbons on the zeolite surface, and it performs additional MC moves to allow the added carbons to find their optimal positions. Proposed moves are accepted or rejected using an energy criterion. The MC process stops when all carbons are sp^2-saturated, and no more surface binding sites are available. The advantage of this approach is that it does not require experimental data and it is relatively computationally inexpensive, so it can be readily extended to other zeolite templates to enable the high-throughput generation of novel ZTCs. More details on the algorithm can be found in *Materials and Methods*. Next we focus on a justification of our method by comparison with the experimental information reported on the (small) subset of ZTCs that have been synthesized so far.

Kim et al. (31) and Parmentier et al. (27) studied the ZTCs templated by the FAU and EMT zeolites using X-ray diffraction (XRD). They found that the carbon-decorated surfaces were well-ordered, but they found disorder in the positions of the carbon atoms. To express this disorder, Kim et al. (31) introduced a model in which ZTC-FAU is described as a network of partially occupied atomic sites. In our ZTC-FAU model, we obtain a similar type of disorder if we compare carbon atom positions over different unit cells or over structures generated using different sets of random numbers. We also observe that the carbon atoms span a consistent surface. In Fig. 1, we compare our ZTC-FAU model with the experimental model, revealing that the carbon atoms of the two models lie on the same surface. Interestingly, Kim et al. (31) found the electron densities in the narrow nanotube-like necks to be more disordered than elsewhere, which they modeled by locating some partially occupied carbon atoms inside the nanotube surfaces, while the rest of the ZTC is completely hollow. In our ZTC-FAU model, we find that some of the necks form fully cylindrical nanotubes while other necks are partially collapsed; in the experimental model, these two structural features are superimposed. In addition, we find that the computed XRD pattern of both our ZTC-FAU and ZTC-EMT structures match well with those of the experiment (30, 31), exhibiting one strong peak for ZTC-FAU and three strong peaks for ZTC-EMT (*SI Appendix*, Fig. S1).

Two further illustrative materials are ZTC-LTA and ZTC-LTL. Kim et al. (31) found that although these ZTCs exhibited zeolite-like crystal morphology and pore order, they could be easily crushed by hand rubbing, and they exhibited photoluminescence when dissolved in *N*-methylpyrrolidone; this was taken as evidence that the carbon was obtained as quantum dots or nanotubes rather than as a strongly bound triply periodic framework. Our ZTC-LTA structure consists of a network of fullerene-type structures linked by single-atom bridges (Fig. 2). These single-atom bridges may explain the physical characteristics experimentally observed, as single-atom bridges are unlikely to be strong enough to withstand forces caused by compression or solvation. Similarly, our ZTC-LTL structure consists of arrays of carbon nanotubes. These observations suggest that zeolite templating might be an alternative synthetic method for producing pure fullerenes—which more typically require postsynthetic purification methods (34)—in much the same way that aluminum oxide templating has been used for producing carbon nanotubes (21).

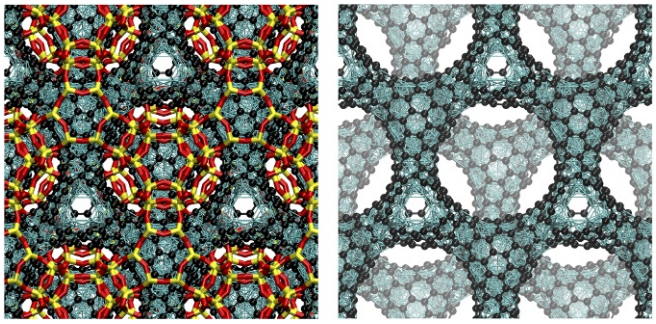

Fig. 1. Similarity between ZTC-FAU synthesized in silico and experiment. Shown is our atomistic model (black carbon atoms), the parent FAU zeolite (red oxygen and yellow silicon atoms), and the XRD-derived model from Kim et al. (31) (cyan lines connecting partially occupied carbon atom positions). *Right* has the zeolite atoms removed for clarity.

Results and Discussion

In the previous section, we have shown that our ZTC-generating method gives very reasonable structural descriptions of the known ZTCs; in this section, we explore other possible ZTCs.

Experimental Accessibility of ZTCs. We show a small subset of the ZTCs we generated using zeolite templates taken from the IZA database (29) in Fig. 2, demonstrating the wide diversity of ZTC topologies possible. From ZTC-LTA and ZTC-LTL, we know that not all zeolite templates will yield ZTCs that remain triply periodic once subject to stress due to the absence of linkages in all three dimensions or due to the presence of weak single-atom bridges formed in zeolite pores of insufficiently large diameter. In addition, zeolites with small pores will be difficult to template since large channels are necessary for the chemical vapor deposition (CVD) precursor to diffuse throughout the zeolite.

We found that ZTCs formed from a parent zeolite with a largest triply periodic free sphere diameter ($D_{f,3p}$) [which we define as the size of the largest spherical probe that can travel through the zeolite's channels in three directions (35)] smaller than about 5 Å either lack linkages in some dimensions, resulting in 1D or 2D carbon structures, or the linkages contain some sort of defect, such as single-atom bridges or flat sheet connectors (Fig. 2, top two rows). Of the ZTCs formed from a parent zeolite with a $D_{f,3p}$ larger than about 5 Å, we were able to find a three-periodic ZTC model that contained none of these defects (Fig. 2, bottom two rows). The cutoff of 5 Å is based on the assumption that atomic carbon is the smallest possible deposition precursor and that no diffusion limitations exist. In practice, however, the precursor can be larger and kinetic barriers to diffusion can restrict access to some pores. Hence, 5 Å should be seen as a lower limit on the $D_{f,3p}$ of zeolites that can be used experimentally as templates for defect-free ZTCs.

We established the finding of a limiting $D_{f,3p}$ around 5 Å by having made ZTCs from a test set of the IZA zeolites, and we then went on to generate ZTCs for nearly all current IZA zeolites with a $D_{f,3p}$ greater than 4.8 Å, going slightly below the limiting value to ensure completeness. We also generated a ZTC for

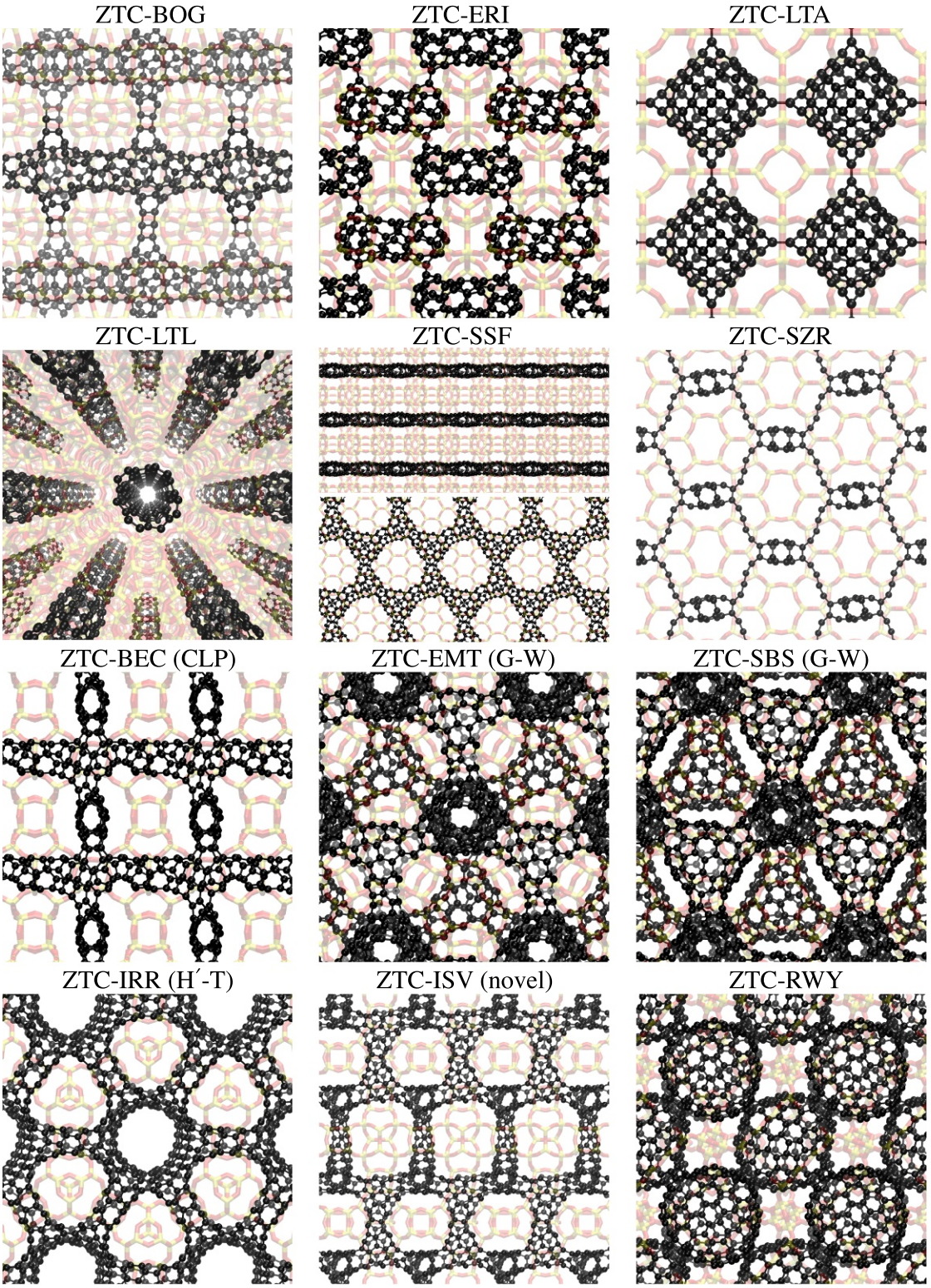

Fig. 2. Library of ZTCs synthesized in silico. Shown is a subset of the ZTC structures (black carbon atoms) and their parent zeolites (red oxygen and yellow silicon atoms). The top two rows of ZTCs were generated from parent zeolites with $D_{f,3p}$ less than 5 Å, and they either lack linkages in some dimensions or they contain linkages with defects; we consider these ZTCs either unlikely to be experimentally synthesizable or unlikely to be stable subject to stress. The bottom two rows of ZTCs were generated from parent zeolites with $D_{f,3p}$ greater than 5 Å, which we propose as experimentally synthesizable and stable structures. The TPMS each structure resembles is given in parentheses. ZTC-RWY does not resemble a TPMS but rather consists of a body-centered cubic packing of fullerenes.

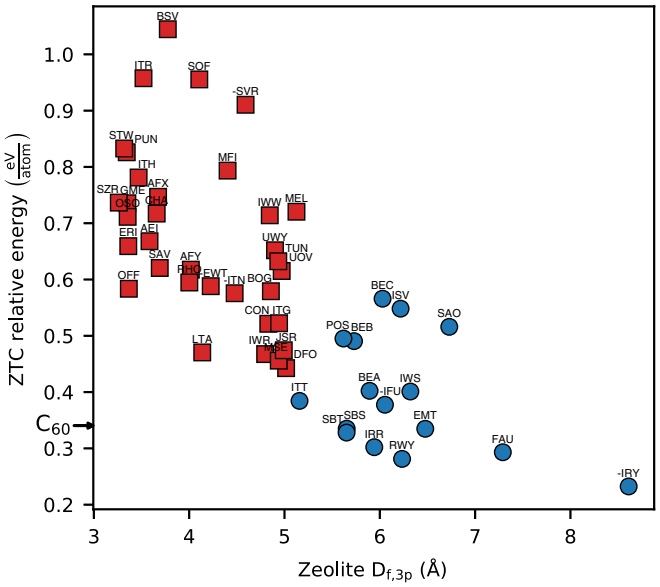

Fig. 3. Per-atom energies of DFT-relaxed three-periodic ZTC models relative to diamond as a function of the parent zeolite's largest triply periodic free sphere diameter ($D_{f,3p}$). The energy of an isolated buckminsterfullerene molecule (C_{60}) is shown as a reference on the *y* axis. Blue circles represent ZTCs free of defects, such as single-atom bridges and flat sheet connectors, while red squares represent ZTCs containing these features. *SI Appendix*, Table S1 contains the information shown in this figure.

beta polymorph B because zeolite beta is one of the few zeolites that has already been shown to generate a ZTC that retains the parent zeolite's structural regularity (22, 30, 31), and zeolite beta is composed of two intergrown structures, polymorphs A and B (36). The only IZA zeolites with a $D_{f,3p}$ greater than 4.8 Å for which we could not produce ZTCs were -CLO, -IFT, and -ITV, with the dash denoting an interrupted framework; these interrupted frameworks have undercoordinated oxygen atoms that extend into the void space of the zeolite and give a less smooth surface for carbon atoms to wrap around.

Next, we relaxed the zeolite-free three-periodic ZTC structures to their local energetic minima using density functional theory (DFT), and we compared their per-atom energies to diamond using the formula $E_{\mathrm{ZTC,relative}} = \frac{E_{\mathrm{ZTC}}}{N_{\mathrm{atoms,ZTC}}} - \frac{E_{\mathrm{diamond}}}{N_{\mathrm{atoms,\ diamond}}}$, where E is the unit cell energy and N_{atoms} is the number of atoms in the unit cell (Fig. 3). We found that the ZTCs free of defects tend to have lower energies, supporting our structural analysis. Several of these ZTCs have energies close to or less than the energy of an isolated buckminsterfullerene molecule.

Finally, we assessed the finite-temperature stability of the ZTCs by performing molecular dynamics (MD) simulations, for which we used the Adaptive Intermolecular Reactive Empirical Bond-Order (AIREBO) force field to allow dynamic breaking and formation of carbon–carbon bonds (37). We summarize the results of these simulations in *SI Appendix*, Table S1. We found that many of the ZTCs containing defects collapsed, broke bonds, or exhibited significant changes to the unit cell parameters. However, almost all of the ZTCs free of defects maintained their structures for several nanoseconds, even at temperatures as elevated as 1,000 K; the only exception was ZTC-IFU, formed from a zeolite with an interrupted framework that, as stated earlier, provides a less smooth surface.

We expect the ZTCs free of defects and that are stable under finite-temperature MD to be experimentally accessible as triply periodic frameworks. The exhaustive list of IZA zeolites that satisfy these thermodynamic and kinetic stability criteria comprises BEA, BEB, BEC, EMT, FAU, IRR, -IRY, ISV, ITT, IWS, POS, RWY, SAO, SBS, and SBT (Table 1). It is encouraging to see that we correctly predict those ZTCs that have already been shown to retain the parent zeolite's structural regularity: namely, ZTC-FAU, ZTC-EMT, and ZTC-beta (22, 30, 31). The remaining zeolites therefore warrant closer attention as templates of potentially synthesizable structures.

Comparison of Experimentally Accessible ZTCs with TPMSs. In prior theoretical work, schwarzites were created by decorating TPMSs with carbon atoms, and so it was known by definition which TPMS a schwarzite resembled (2–6). We must instead associate a ZTC with a TPMS a posteriori. The carbon atoms of a ZTC lie on a surface (38)—the ZTC surface—and here we find the TPMS that most closely resembles this surface.

Of the 15 ZTCs we suggest as experimentally accessible, the majority form surfaces that partition space into two disjoint labyrinths that can be described by the nets running through them, as is common in the study of TPMSs (Fig. 4) (16–18). Only ZTC-RWY does not form a surface that bounds two labyrinths, with the structure instead consisting of a body-centered cubic packing of fullerenes (Fig. 2); we focus on the remaining 14 ZTCs. We associate each of these 14 ZTCs with the TPMS that could be traced by the same labyrinth nets in a matching lattice system. We obtained the two ZTC labyrinth nets in a manner that provides an unambiguous assignment (see *Materials and Methods* for details). Depositing the carbon atoms on the zeolite surface will leave the zeolite atoms in one of the two labyrinths defined by that surface (39). We refer to the ZTC labyrinth that contained the zeolite atoms before their removal as the zeolite labyrinth, with the other labyrinth referred to as the void labyrinth (Fig. 4).

One way to illustrate the similarity between a ZTC surface and its associated TPMS is by performing a geometrical transformation, numerically minimizing the area of the ZTC surface subject to constant volume constraints. By gradually varying the volumes of the two labyrinths until their ratio matches that of the labyrinths defined by the corresponding TPMS, the relation

Table 1. Topology and symmetry of the experimentally accessible ZTCs and their parent zeolites

Zeolite	Zeolite's space group	ZTC's zeolite labyrinth net	ZTC's void labyrinth net	Labyrinth nets' genus	TPMS resembling ZTC
RWY	$Im\bar{3}m$	**nbo***	**bcu***	4*	I-WP*
FAU	$Fd\bar{3}m$	**dia**	**dia**	3	D
EMT	$P6_3/mmc$	**lon**	**gra**	5	G-W
-IRY	$P6_3/mmc$	**lon**	**gra**	5	G-W
SBS	$P6_3/mmc$	**lon**	**gra**	5	G-W
IRR	P6/mmm	**bnn**	**hex**	4	H′-T
ITT	P6/mmm	**bnn**	**hex**	4	H′-T
SBT	$R\bar{3}m$	**dia**†	**dia**†	3	rPD
IWS	I4/mmm	4,6T585	**crb**	5	Novel
POS	$P4_2/mnm$	**cds**†	**cds**†	3	CLP‡
BEC	$P4_2/mmc$	**cds**	**cds**	3	CLP
ISV	$P4_2/mmc$	sqc145	**tfi**	5	Novel
SAO	$I\bar{4}m2$	**dia**†	**tfa**	3	tD
BEA	$P4_122$	**ths**†	**ths**†	3	tD
BEB	C2/c	**ths**†	**ths**†	3	mDCLP

*The model ZTC's connecting tunnels are pinched off, disrupting the labyrinth and forming a structure consisting of a body-centered cubic packing of fullerenes. Here we describe the surface that would have formed if the pinching off had not occurred and the cages were instead connected.
†Not the maximum-symmetry embedding of the net.
‡The CLP TPMS has the $P4_2/mmc$ space group, which is a minimal supergroup of the POS zeolite's $P4_2/mnm$ space group. All other identified TPMSs in the table have the same space group as the parent zeolite.

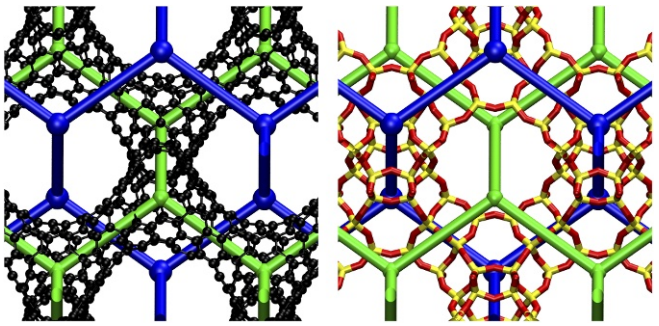

Fig. 4. Labyrinth nets of ZTC-FAU. (*Left*) One of our ZTC-FAU models (black carbon atoms), and (*Right*) its parent FAU zeolite (red oxygen and yellow silicon atoms), both shown with the ZTC's **dia** zeolite labyrinth net (blue) and the ZTC's **dia** void labyrinth net (green) (40).

between the surfaces becomes apparent. We demonstrate this process in Fig. 5 for ZTC-FAU and in *SI Appendix*, Fig. S2 for ZTC-EMT.

We show the TPMSs we associate with each of the experimentally accessible ZTCs in Table 1, where it can be seen that many of the ZTCs resemble known TPMSs. We identify ZTC-FAU as resembling the Schwarz D TPMS and ZTC-EMT as resembling the Schoen G-W TPMS (originally referred to as g–g′) (16), with the latter TPMS also resembling ZTC-IRY and ZTC-SBS. ZTC-EMT and ZTC-SBS are illustrated in Fig. 2, where the structural similarities between these two ZTCs are readily apparent, making evident the reason for their associations with the same TPMS. Nonetheless, it is clear that the two ZTCs are not identical: The two surfaces have different labyrinth volume ratios and unit cell parameter to carbon–carbon bond length ratios, and the carbon networks are distinct; for example, they are composed of unequal fractions of hexagonal, heptagonal, and octagonal rings with varying degrees of strain. These disparities will lead to distinctive electrical and mechanical properties, giving materials with different performances for select applications.

Other TPMSs we have found to resemble ZTCs include Schwarz CLP (41), Schoen H′-T (16), Schoen tD (16, 42), rPD of Koch and Fischer (42), and mDCLP of Fogden and Hyde (43), the last three of which are lower symmetry variants of the Schwarz D TPMS. To the best of our knowledge, TPMSs with the labyrinth nets of ZTC-IWS and ZTC-ISV have not been reported in the literature, which may be because they are of the less well-studied nonbalanced surfaces (a TPMS that divides space into two congruent labyrinths is known as a balanced TPMS, whereas a nonbalanced TPMS has noncongruent labyrinths) (44, 45). Since we have made atomistic models of ZTCs from all known noninterrupted zeolites with sufficiently large $D_{f,3p}$, to the best of our knowledge the TPMSs discussed in this work represent an exhaustive list of all schwarzites that can be made by templating the presently known zeolites with carbon.

Rational Design of Schwarzite Templates. So far, we have shown how to determine which schwarzite will be generated by templating a given zeolite. Equally interesting is the inverse problem: determining which template will produce a schwarzite resembling a given TPMS. If a TPMS of, say, type CLP is desired, Table 1 can be consulted to find that zeolites POS and BEC can be used as templates. However, if the TPMS is not in Table 1, a novel material would be needed. Fortunately, new zeolites are continuously being synthesized, and the ability to rationally design synthetic methods to achieve desired zeolites is beginning to become available (46–48). Furthermore, one need not restrict oneself to zeolites as multiple new material classes are being developed for use as hard-templates (20, 23).

To obtain some insights into the types of new structures that can be generated, it is interesting to consider the databases of hypothetical zeolites that have been developed to guide the discovery of new zeolites. In this work, we used Treacy and Foster's silver hypothetical zeolite database, which contains 1,270,921 structures with energies within 48.2 kJ mol_{Si}^{-1} of α-quartz, and Deem's SLC hypothetical zeolite database, which contains 331,172 structures with energies within 30 kJ mol_{Si}^{-1} of α-quartz, with 48.2 kJ mol_{Si}^{-1} and 30 kJ mol_{Si}^{-1} being each database creator's respective criterion for a structure's experimental accessibility (49, 50). In principle, we can solve the inverse problem by generating the ZTCs for all these hypothetical zeolites and tabulating the corresponding TPMSs, similarly to our approach for the known zeolites, but the large number of structures makes this impractical.

To avoid this enormous computational effort, we can significantly filter down the hypothetical zeolite databases. Namely, we can restrict the search to zeolites with $D_{f,3p}$ larger than 5 Å and

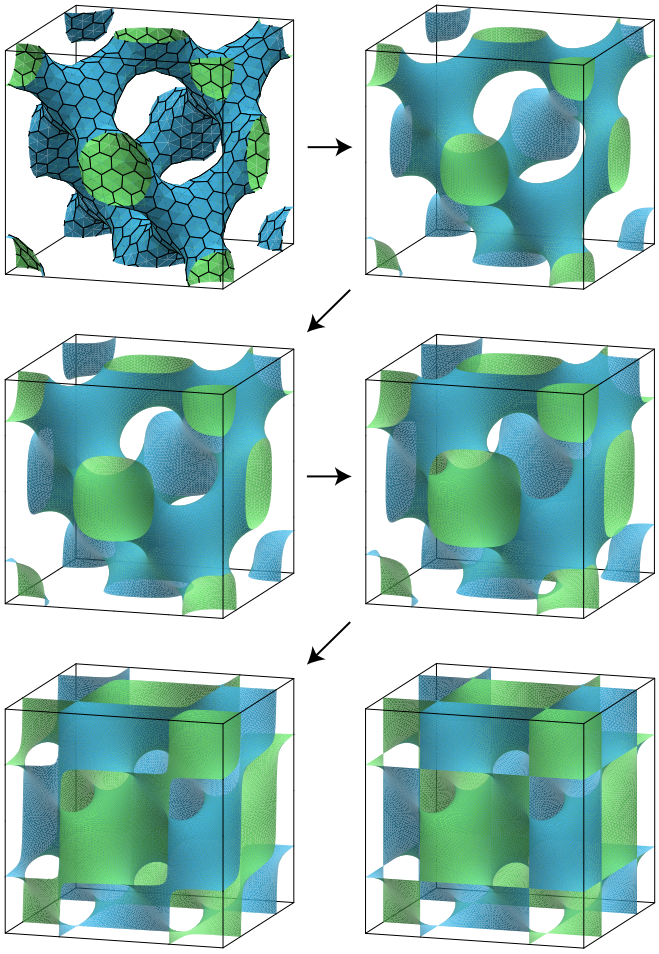

Fig. 5. Numerical minimization of ZTC-FAU's surface area. The process begins with the vertices of the surface defined by the carbon atoms and triangulation of the faces (first image), followed by further refinement of the triangulation by subdividing the original triangles and minimizing the surface area subject to a constant volume constraint (second image). The ratio of the two labyrinths' volumes in the constraint is slowly varied while continuing to minimize the surface area (third and fourth images) until it is in unity (fifth image), equal to that of the Schwarz D TPMS. The resulting surface is visually very similar to the Schwarz D TPMS (final image). The side of the surface touching the ZTC's zeolite labyrinth is colored blue, and the side touching the ZTC's void labyrinth is colored green. See also *SI Appendix*, Movie S1.

which have the same space group as the target TPMS. The latter filter comes from an expectation that the space group of the TPMS associated with a ZTC should either be identical with or a supergroup of the space group of the parent zeolite, an expectation that is consistent with our findings given in Table 1. [We note that a balanced TPMS can be described by a group–subgroup pair of space groups (44); we refer to the subgroup that describes the symmetry of the oriented surface—that is, the space group that distinguishes the surface's two sides.]

However, a space group does not uniquely define a TPMS, and so the target TPMS would not be the only one that could form from zeolites with the same space group. To understand which structures are more likely to be formed, we must consider the topology of TPMSs in addition to their symmetry. A useful measure of a surface's topology is its genus, which is the number of handles the surface contains. For example, known TPMSs with space group $Pm\bar{3}m$ include the P, C(P), C(P)b, C(P)a, Pb, and Pa TPMSs of genus 3, 9, 15, 19, 21, and 25, respectively (45). Higher genus surfaces have more tunnels in the unit cell, the formation of which require correspondingly more channels in the unit cell of the zeolite template. The bond length and angle constraints of zeolites prevent a large number of channels without requiring a larger unit cell, yet zeolites tend to be very regular materials with high symmetry and small unit cells. Thus, we would expect zeolites to be more likely to form low-genus TPMSs. Indeed, we observe that the TPMSs from all known zeolites have a low genus of 3, 4, or 5 (Table 1). Hence, provided that the target TPMS is of sufficiently low genus, we expect to be able to solve the inverse problem within the zeolite material class.

To illustrate these points, let us attempt to solve the inverse problem for a set of target TPMSs. A natural choice of targets is the "minimal minimal surfaces," so called because they have genus 3, the smallest possible genus for a TPMS (18). Only five minimal minimal surfaces are known; these are the Schwarz D, CLP, H, and P TPMSs, and the Schoen G TPMS (deformations of which admit lower symmetry variants like the tD, mDCLP, and rPD TPMSs) (16, 18, 41). By examining Table 1, we see that there already exist zeolites that can generate the D and CLP TPMSs, but corresponding zeolites are not present for the H, P, and G TPMSs. It is an interesting question as to whether all of the minimal minimal surfaces can be generated using zeolite templates, since these surfaces play a relevant role in the science of materials (17, 18), and they have been examined as schwarzites in the most depth (2–6). As a motivating example, Qin et al. (51) have shown that a schwarzite resembling the Schoen G TPMS has interesting properties, but they could not suggest how to synthesize it; here, we demonstrate how to find a material that would template it.

The first step is to seek zeolites with a space group matching the desired surface (e.g., $P\bar{6}m2$ for the H TPMS) that also must have sufficiently large $D_{f,3p}$. Out of the 1.6 million hypothetical zeolite structures, we found 476 with the $P\bar{6}m2$ space group, of which 23 had a $D_{f,3p}$ greater than 5.0 Å. We evaluated the first six materials for which our ZTC-generating algorithm converged on final structures, and we found that five of these ZTCs had **hms** labyrinth nets and thus resembled the H TPMS, while one instead resembled the G-W TPMS (Fig. 6 and *SI Appendix*, Table S1). The ZTC resembling the G-W TPMS exhibits the same increase in symmetry from zeolite to TPMS as was observed with ZTC-POS (the G-W TPMS has space group $P6_3/mmc$, which is a supergroup of $P\bar{6}m2$); this result demonstrates that it is expedient to first determine the likely labyrinth nets by generating the accessible zeolite surface using inexpensive geometric methods (35) before generating the full atomistic ZTC structure.

Similarly, we can find corresponding zeolites for the remaining P and G TPMSs by matching their respective space groups, $Pm\bar{3}m$ and $I4_132$. Out of the hypothetical zeolite structures, we found 23 and 4 with these space groups, of which 4 and 2 had a $D_{f,3p}$ greater than 5.0 Å. From these, the first materials for which our ZTC-generating algorithm converged on a final structure did resemble the P and G TPMSs, having **pcu** and **srs** labyrinth nets (Fig. 6 and *SI Appendix*, Table S1). Thus, we see that we are indeed capable of solving the inverse problem.

Concluding Remarks

In this work, we have developed an in silico method to generate ZTCs from any zeolite structure. Our method correctly describes the structures of the known ZTCs and allows us to present a complete library of ZTCs that ought to be synthesizable from known zeolites; this library should serve to guide experimentalists and to provide computational scientists with realistic atomistic models. Furthermore, we have shown how ZTCs can be associated with TPMSs, linking the research topics of ZTCs and schwarzites. Finally, we have demonstrated how to find template materials that would yield a desired schwarzite.

An interesting observation is that all known zeolites form low-genus surfaces, while in the databases of hypothetical zeolites one can find structures that give surfaces with relatively high genus. For example, Treacy and Foster's hypothetical zeolite 225_6_1852 has one of the largest unit cell volumes (49), and the genus of the corresponding ZTC surface would be 11. In fact, one can envision generating hypothetical zeolite structures with even higher genus by simply replicating an existing zeolite's unit cell and then breaking the symmetry. A tempting speculation is that a large genus ZTC surface might itself be an indication of the difficulty of synthesizing its parent zeolite. Some connection might be made here between ZTCs and the structure-directing agents (SDAs) that frequently direct zeolite synthesis. These SDAs sometimes act as soft templates around which zeolites crystallize (52), making ZTCs a sort of inverse–inverse material. The self-assembly of surfactants has also been described using the TPMS concept (17). Thus, the synthesis of high-genus TPMSs might require the synthesis of zeolites that in turn require the use of SDAs that self-assemble into complicated structures.

By focusing on the striking similarities between ZTCs and schwarzites, we have found that theories about TPMSs give insight into ZTCs, useful for such problems as how to select a zeolite template to obtain a microporous ordered carbon with a particular pore topology. Although schwarzites have been a purely hypothetical concept, our work suggests that ZTCs are schwarzites incarnate. One conceivable difference between these material classes is that the carbon atoms of ZTCs deviate from the TPMS surface, whereas schwarzites were generated by placing carbon atoms exactly on the TPMS surface. However, this difference is in quantity rather than in quality, as energetic relaxation of the schwarzites also causes a deviation from the true TPMS (3, 5). Finally, we note that past works hypothesized carbon schwarzites without regard to the method by which they can be synthesized, assuming that structures with low energies, high stability, and high symmetry will eventually be found. In contrast, our ZTC structures have been made with a direct synthetic pathway in mind, which may lead to more success in guiding experimental efforts.

Materials and Methods

ZTC generation was performed using an in-house MC code. All known zeolite structures were taken from the IZA database (29); two exceptions to this were FAU, which was taken as the zeolite atoms in the XRD-derived structure of the carbon-loaded zeolite from Kim et al. (31) to allow for better visual comparison with their experimental model, and BEB, which was taken from the Inorganic Crystal Structure Database (53) entry of Martínez-Iñesta et al. (54). "BEB" refers to polymorph B of zeolite beta, which is composed of two intergrown structures [polymorph A

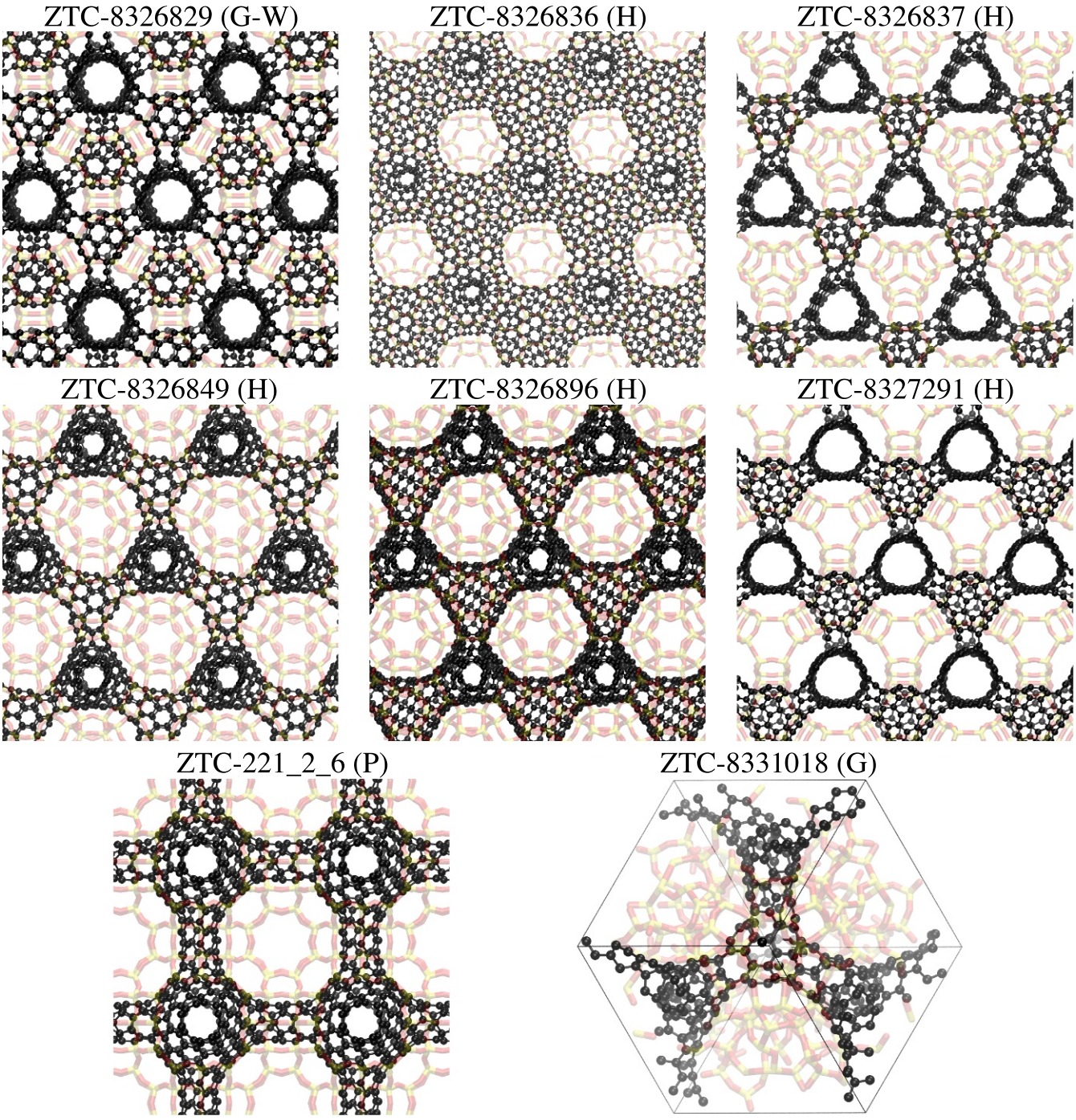

Fig. 6. ZTCs synthesized in silico from hypothetical zeolites with the same space groups as the H, P, and G minimal minimal surfaces. Shown are the ZTC structures (black carbon atoms) along with their parent zeolites (red oxygen and yellow silicon atoms). The TPMS each structure resembles is given in parentheses. The top two rows of ZTCs were generated from zeolites with space group $P\bar{6}m2$, ZTC-221_2_6 was generated from a zeolite with space group $Pm\bar{3}m$, and ZTC-8331018 was generated from a zeolite with space group $I4_132$. Zeolite 221_2_6 was taken from Treacy and Foster's silver hypothetical zeolite database, and the other zeolites were taken from Deem's SLC hypothetical zeolite database (49, 50).

is referred to as BEA, but polymorph B lacks an IZA assignment (29)]. The hypothetical zeolite structures were taken from Treacy and Foster's silver hypothetical zeolite database and Deem's SLC hypothetical zeolite database (49, 50).

The generation of a ZTC begins with a seed of four carbon atoms (a central atom bonded to three neighbors) placed in the zeolite's pore space. Two types of MC moves were then attempted: moves that insert–delete carbon atoms and moves that change the carbon bonding network. Insertion moves were performed by first selecting an existing undercoordinated carbon atom and, depending on the coordination of the selected carbon atom, adding either one or two new carbon atoms. The new carbon atoms were placed in an empty space in a shell around the selected carbon atom and were bonded to this atom. Additional bonds were added between the inserted atoms and other neighboring undercoordinated carbon atoms. Deletion moves were done by first selecting an existing undercoordinated carbon atom and removing the atom and its one or two bonds; if the deleted atom had two bonds, a new bond was created between the two atoms to which it was formerly bonded.

Moves that change the bonding network include bond propagation, bond disassociation, and bond switching. The bond propagation move involves three carbon atoms, two that are bonded and a nonbonded neighbor. The bond between the two carbon atoms is deleted, and a new bond is placed between one of them and the neighbor. The bond disassociation move is deletion of a bond. The bond switching move involves four neighboring carbon atoms, between which the bonding network is reorganized.

In our MC procedure, we randomly select to insert, delete, propagate, or disassociate, and each trial move includes a subsequent energetic relaxation of all carbon atoms. This relaxation involves finding the optimum bonding network by bond switching moves, followed by a conjugate-gradient relaxation of the carbon atomic positions. The overall trial move is then accepted with probability $\min[1, \exp(-\beta\Delta E)]$, where ΔE is the energy difference between the old structure and the relaxed trial structure. To surmount energetic barriers, it is important to set the effective temperature sufficiently high (24); we found 2,000 K to work well. The MC simulation was ended when all carbon atoms had three bonds and no significant reduction in energy was being observed. Changing the temperature and other variables in our algorithm does not affect the overall surface formed.

The valence force field of Lee and Hwang (55) was used to model carbon–carbon interactions. The exact parameters are from a slightly improved set provided by Lee and Hwang: $r_0 = 1.41239$ Å, $\theta_0 = 120^\circ$, $k_r = 20.559$ eV, $k_\theta = 3.5125$ eV, $k_\phi = 0.561735$ eV, and $k_\varphi = 0.0081$ eV. This force field was chosen because it was designed specifically for sp^2-hybridized carbon, and it features an energetic penalty for misalignment of neighboring π orbitals, making it both more descriptive of ZTC carbon atoms and less computationally expensive than the general-purpose AIREBO force field (37, 55, 56). (We initially attempted to use the AIREBO force field to model carbon–carbon interactions in a GCMC simulation, but we found that with no disincentive against the formation of a nonplanar structure, and with the carbon bonding strength orders of magnitude greater than the weak physisorption interactions between the carbon atoms and the zeolite, there was a very small range of acceptable chemical potentials in which carbon neither undertemplates the zeolite surface nor fills in the zeolite's void space.) Carbon–framework interactions were described by Lennard–Jones interactions using Universal force-field parameters with Lorentz–Berthelot mixing rules and a simply truncated cutoff of 7.0 Å (57).

Our criteria for considering a ZTC experimentally accessible included the absence of defects such as single-atom bridges and flat sheet connectors. For some zeolites, we noticed that a ZTC model would contain defective features on some generations and be free of them on others, indicating a free energy barrier to assembly. Thus, we chose our criterion to be that at least one model free of these features had to be obtained for a ZTC to be considered experimentally accessible, and we generated additional ZTC models in borderline cases. For example, zeolites IRR, IWS, and SBT all gave defect-free ZTCs on a second attempt, while we could not obtain defect-free ZTCs for zeolites JSR, SVR, and TUN over several attempts. Zeolites with $D_{f,3p}$ close to 5 Å for which we were unable to find a defect-free ZTC model might be obtainable with a large number of trials, but since ZTCs would be difficult to synthesize from these templates due to CVD precursor diffusion limitations, we considered them less likely to be experimentally accessible, and so we chose to focus on ZTCs formed from zeolites with $D_{f,3p}$ above 5 Å.

DFT calculations were performed with CP2K version 4.1 (58, 59), using the PBE density functional (60) and Grimme's D3 dispersion correction (61). Integration over the Brillouin zone was carried out over a Γ-centered Monkhorst–Pack grid, where the number of subdivisions along each reciprocal lattice vector was given by $\max(1, \text{floor}(25|b_i| + 0.5))$, where $|b_i|$ is the norm of the ith reciprocal lattice vector; this formula gave a $2 \times 2 \times 2$ grid for ZTC-FAU, which was found to be sufficient for k-point convergence. We used double-ζ shorter range Gaussian basis sets (62), plane-wave basis sets cut off at 300 Ry, and the Goedecker–Teter–Hutter pseudopotentials (63, 64). The wavefunction energy convergence criterion was set to 1×10^{-6}, and the atomic positions, unit cell shape, and unit cell volume were optimized simultaneously until all forces were smaller than 4.5 $E_h a_0^{-1}$. The buckminsterfullerene energy calculation was conducted by placing a single molecule in a cubic unit cell of length 40 Å to approximate isolation.

MD simulations were conducted with the August 11, 2017 release of the LAMMPS simulation software package (65). The AIREBO (37) force field was used with no charges and a cutoff of 10.2 Å. The ZTC unit cells were replicated to ensure that the three perpendicular widths of the simulation boxes were all greater than 20.4 Å. The timestep used was 1 fs. The equations of motion were integrated with a standard velocity Verlet algorithm using half-step velocity calculations. Following minimization of the system energy by adjusting atomic coordinates, the MD simulation was run for 1 ns in the canonical (NVT) ensemble, an additional 1 ns in the isothermal–isobaric (NPT) ensemble with only the three lattice constants allowed to change, and a final 1 ns in the NPT ensemble with the three lattice constants and the three angles between them allowed to change. A Nosé–Hoover thermostat was used with a time damping constant of 100 fs and a total of three chained thermostats. A Nosé–Hoover barostat was used with a time damping constant of 1,000 fs, and it was thermostated with a chain of three thermostats.

Topological analysis was conducted with ToposPro version 5.3.0.2 (66). The two nets that describe the ZTCs' two labyrinths were obtained by taking the natural tiling of the parent zeolite (67), determining the dual net of this tiling using ToposPro (66), and decomposing the dual net into two interpenetrated subnets by deleting edges that cross the ZTC surface. In some cases, this construction leads to a labyrinth net that is disconnected, and the missing edges were added. Subsequently, both labyrinth nets were simplified in the following manners. When an edge was found to be incident to two coordinated vertices, the edge was contracted. When a net was found to contain a strong ring [a cycle that is not a sum of smaller cycles (66)] that bounds a face wholly contained within its labyrinth, the ring was replaced by a single vertex located at the ring's centroid, which was connected to the vertices that were formerly connected to the ring. Similarly, when a net was found to contain several strong rings with shared edges that each bounds a face wholly contained within their labyrinth, the set of rings was replaced by a single vertex as described above; for example, six strong rings making up the edges of a cube were replaced by the cube's centroid, and two strong rings whose sum forms the boundary of a quadrilateral were replaced by the quadrilateral's centroid. The resulting nets were assigned names according to the Reticular Chemistry Structure Resource (RCSR) nomenclature when available (e.g., **dia**, **lon**) (40), Epinet nomenclature otherwise (sqc145) (68), and ToposPro's Topological Types Database (TTD) nomenclature when neither of the first two were available (4,6T585) (69). Our method provides an unambiguous assignment of the nets, and it captures the nets' symmetry embeddings. In general, different nets can be used to trace a given labyrinth (18), so although our method gives a valid choice of nets that captures the geometry of the labyrinths well for our purpose, other choices can equally well lie in the labyrinth; for example, ZTC-SAO's void labyrinth net can be properly traced by a $I\bar{4}m2$ embedding of both the **tfa** and **dia** nets, and the multiple labyrinths described by the **ths** net can also be traced by the **dia** net.

The $D_{f,3p}$s of zeolites were calculated using Zeo++ version 0.3 with silicon and oxygen atomic radii both set to 1.35 Å for consistency with the sphere diameters calculated in the IZA database (29, 35). Powder XRD patterns were calculated with Mercury version 3.9 using the Cu $K\alpha_1$ wavelength of 1.540 56 Å (70). Numerical surface area minimization was conducted with the Surface Evolver version 2.70 (71), for which input files of the Schwarz D and Schoen G-W TPMSs were taken from Ken Brakke's website (72).

We have made the following files accessible with the Open Science Framework (doi.org/10.17605/OSF.IO/ZHDB2) and with the Materials Cloud (doi.org/10.24435/materialscloud:2018.0013/v1): structure files of all nonrelaxed and DFT-relaxed ZTCs, a ToposPro database that contains the nets of all ZTCs in Table 1, and input files we used with CP2K, LAMMPS, and Surface Evolver.

ACKNOWLEDGMENTS. We thank the responders on the LAMMPS mailing list for eliminating bugs in the AIREBO force field implementation (Steven J. Plimpton, Axel Kohlmeyer, Markus Hoehnerbach, Cyril Falvo, and Richard Berger were particularly helpful), Ben Slater for helpful discussions on carbon allotropes and TPMSs, and Peter Boyd for helpful discussions on crystal topology. This research was supported as part of the Center for Gas Separations Relevant to Clean Energy Technologies, an Energy Frontier Research Center funded by the US Department of Energy, Office of Science, Basic Energy Sciences under Award DE-SC0001015. This research used resources of the National Energy Research Scientific Computing Center, a DOE Office of Science User Facility supported by the Office of Science of the US Department of Energy under Contract DE-AC02-05CH11231. Y.L. thanks the ShanghaiTech University Research Startup Fund and the high-performance computing platform of ShanghaiTech University for support. S.M.M. acknowledges funding by the Deutsche Forschungsgemeinschaft (DFG, Priority Program SPP 1570). S.B. acknowledges funding by the National Center of Competence in Research (NCCR) Materials' Revolution: Computational Design and Discovery of Novel Materials ("MARVEL") of the Swiss National Science Foundation (SNSF). R.M. acknowledges support from an NSF Graduate Research Fellowship under Grant DGE 1106400. I.A.B. thanks the European Commission for support under the Graphene Flagship program (Contract NECT-ICT-604391). B.S. acknowledges support from the European Research Council (ERC) under the European Union's Horizon 2020 research and innovation programme (Grant Agreement 666983, MaGic).

1. Hoffmann R, Kabanov AA, Golov AA, Proserpio DM (2016) Homo citans and carbon allotropes: For an ethics of citation. *Angew Chem Int Ed Engl* 55:10962–10976.
2. Mackay AL, Terrones H (1991) Diamond from graphite. *Nature* 352:762.
3. Lenosky T, Gonze X, Teter M, Elser V (1992) Energetics of negatively curved graphitic carbon. *Nature* 355:333–335.
4. Vanderbilt D, Tersoff J (1992) Negative-curvature fullerene analog of C_{60}. *Phys Rev Lett* 68:511–513.
5. Terrones H, Mackay AL (1992) The geometry of hypothetical curved graphite structures. *Carbon* 30:1251–1260.
6. O'Keeffe M, Adams GB, Sankey OF (1992) Predicted new low energy forms of carbon. *Phys Rev Lett* 68:2325–2328.
7. Huang MZ, Ching WY, Lenosky T (1993) Electronic properties of negative-curvature periodic graphitic carbon surfaces. *Phys Rev B* 47:1593–1606.
8. Terrones H, Terasaki M (2003) Curved nanostructured materials. *New J Phys* 5:126.
9. Park N, et al. (2003) Magnetism in all-carbon nanostructures with negative Gaussian curvature. *Phys Rev Lett* 91:237204.
10. Lherbier A, Terrones H, Charlier J-C (2014) Three-dimensional massless Dirac fermions in carbon schwarzites. *Phys Rev B* 90:125434.
11. Odkhuu D, et al. (2014) Negatively curved carbon as the anode for lithium ion batteries. *Carbon* 66:39–47.
12. Ewels CP, et al. (2015) Predicting experimentally stable allotropes: Instability of pentagraphene. *Proc Natl Acad Sci USA* 112:15609–15612.
13. Bourgeois LN, Bursill LA (1997) High-resolution transmission electron microscopic study of nanoporous carbon consisting of curved single graphitic sheets. *Philos Mag A* 76:753–768.
14. Barborini E, et al. (2002) Negatively curved spongy carbon. *Appl Phys Lett* 81: 3359–3361.
15. Townsend SJ, Lenosky TJ, Muller DA, Nichols CS, Elser V (1992) Negatively curved graphitic sheet model of amorphous carbon. *Phys Rev Lett* 69:921–924.
16. Schoen AH (1970) Infinite periodic minimal surfaces without self-intersections (NASA Electronics Research Center, Cambridge, MA), Technical Report NASA TN D-5541, C-98.
17. Andersson S, Hyde ST, Larsson K, Lidin S (1988) Minimal surfaces and structures: From inorganic and metal crystals to cell membranes and biopolymers. *Chem Rev* 88:221–242.
18. de Campo L, Delgado-Friedrichs O, Hyde ST, O'Keeffe M (2013) Minimal nets and minimal minimal surfaces. *Acta Crystallogr Sect A* A69:483–489.
19. Xia Y, Yang Z, Mokaya R (2010) Templated nanoscale porous carbons. *Nanoscale* 2:639–659.
20. Inagaki M, Orikasa H, Morishita T (2011) Morphology and pore control in carbon materials via templating. *RSC Adv* 1:1620–1640.
21. Nishihara H, Kyotani T (2012) Templated nanocarbons for energy storage. *Adv Mater* 24:4473–4498.
22. Nishihara H, Kyotani T (2012) Zeolite-templated carbon—Its unique characteristics and applications. *Novel Carbon Adsorbents*, ed Tascón JM (Elsevier, Amsterdam), pp 295–322.
23. Malgras V, et al. (2015) Templated synthesis for nanoarchitectured porous materials. *Bull Chem Soc Jpn* 88:1171–1200.
24. Roussel T, et al. (2007) Experimental and atomistic simulation study of the structural and adsorption properties of faujasite zeolite-templated nanostructured carbon materials. *J Phys Chem C* 111:15863–15876.
25. Roussel T, Bichara C, Gubbins KE, Pellenq RJ-M (2009) Hydrogen storage enhanced in Li-doped carbon replica of zeolites: A possible route to achieve fuel cell demand. *J Chem Phys* 130:174717.
26. Nueangnoraj K, et al. (2013) Formation of crosslinked-fullerene-like framework as negative replica of zeolite Y. *Carbon* 62:455–464.
27. Parmentier J, Gaslain FOM, Ersen O, Centeno TA, Solovyov LA (2014) Structure and sorption properties of a zeolite-templated carbon with the EMT structure type. *Langmuir* 30:297–307.
28. Nishihara H, et al. (2018) Graphene-based ordered framework with a diverse range of carbon polygons formed in zeolite nanochannels. *Carbon* 129:854–862.
29. Baerlocher C, McCusker LB, Database of zeolite structures. Available at www.iza-structure.org/databases. Accessed October 9, 2017.
30. Gaslain FOM, Parmentier J, Valtchev VP, Patarin J (2006) First zeolite carbon replica with a well resolved X-ray diffraction pattern. *Chem Commun* 0:991–993.
31. Kim K, et al. (2016) Lanthanum-catalysed synthesis of microporous 3d graphene-like carbons in a zeolite template. *Nature* 535:131–135.
32. Nishihara H, et al. (2009) A possible buckybowl-like structure of zeolite templated carbon. *Carbon* 47:1220–1230.
33. Roussel T, Bichara C, Pellenq RJ-M (2005) Selenium and carbon nanostructures in the pores of $AlPO_4$-5. *Adsorption* 11:709–714.
34. Jariwala D, Sangwan VK, Lauhon LJ, Marks TJ, Hersam MC (2013) Carbon nanomaterials for electronics, optoelectronics, photovoltaics, and sensing. *Chem Soc Rev* 42:2824–2860.
35. Willems TF, Rycroft CH, Kazi M, Meza JC, Haranczyk M (2012) Algorithms and tools for high-throughput geometry-based analysis of crystalline porous materials. *Microporous Mesoporous Mater* 149:134–141.
36. Treacy MMJ, Newsam JM (1988) Two new three-dimensional twelve-ring zeolite frameworks of which zeolite beta is a disordered intergrowth. *Nature* 332:249–251.
37. Stuart SJ, Tutein AB, Harrison JA (2000) A reactive potential for hydrocarbons with intermolecular interactions. *J Chem Phys* 112:6472–6486.
38. Mackay AL (1995) Flexicrystallography: Curved surfaces in chemical structures. *Curr Sci* 69:151–161.
39. Brenner S, McCusker LB, Baerlocher C (1997) Using a structure envelope to facilitate structure solution from powder diffraction data. *J Appl Crystallogr* 30:1167–1172.
40. O'Keeffe M, Peskov MA, Ramsden SJ, Yaghi OM (2008) The reticular chemistry structure resource (RCSR) database of, and symbols for, crystal nets. *Acc Chem Res* 41:1782–1789.
41. Schwarz HA (1890) *Gesammelte Mathematische Abhandlungen* (Springer, Berlin).
42. Koch E, Fischer W (1988) On 3-periodic minimal surfaces with non-cubic symmetry. *Z Kristallogr* 183:129–152.
43. Fogden A, Hyde ST (1992) Parametrization of triply periodic minimal surfaces. II. regular class solutions. *Acta Crystallogr Sect A* A48:575–591.
44. Fischer W, Koch E (1996) Spanning minimal surfaces. *Phil Trans R Soc A* 354: 2105–2142.
45. Lord EA, Mackay AL (2003) Periodic minimal surfaces of cubic symmetry. *Curr Sci* 85:346–362.
46. Moliner M, Rey F, Corma A (2013) Towards the rational design of efficient organic structure-directing agents for zeolite synthesis. *Angew Chem Int Ed* 52:13880–13889.
47. Pophale R, Daeyart F, Deem MW (2013) Computational prediction of chemically synthesizable organic structure directing agents for zeolites. *J Mater Chem A* 1:6695–6970.
48. Zimmermann NER, Haranczyk M (2016) History and utility of zeolite framework-type discovery from a data-science perspective. *Cryst Growth Des* 16:3043–3048.
49. Treacy MMJ, Rivin I, Balkovsky E, Randall KH, Foster MD (2004) Enumeration of periodic tetrahedral frameworks. II. polynodal graphs. *Microporous Mesoporous Mater* 74:121–132.
50. Pophale R, Cheeseman PA, Deem MW (2011) A database of new zeolite-like materials. *Phys Chem Chem Phys* 13:12407.
51. Qin Z, Jung GS, Kang MJ, Buehler MJ (2017) The mechanics and design of a lightweight three-dimensional graphene assembly. *Sci Adv* 3:e1601536.
52. Čejka J, Morris RE, Nachtigall P, eds (2017) *Zeolites in Catalysis: Properties and Applications*, Number 28 in Catalysis (Royal Society of Chemistry, Cambridge, UK).
53. Belsky A, Hellenbrandt M, Karen VL, Luksch P (2002) New developments in the inorganic crystal structure database (ICSD): Accessibility in support of materials research and design. *Acta Crystallogr Sect B* 58:364–369.
54. Martínez-Iñesta MM, Peral I, Proffen T, Lobo RF (2005) A pair distribution function analysis of zeolite beta. *Microporous Mesoporous Mater* 77:55–66.
55. Lee S, Hwang GS (2011) Valence force field-based Monte Carlo bond-rotation method for the determination of sp^2 bonded carbon structures. *J Appl Phys* 110:093524.
56. Perebeinos V, Tersoff J (2009) Valence force model for phonons in graphene and carbon nanotubes. *Phys Rev B* 79:241409.
57. Rappe AK, Casewit CJ, Colwell KS, Goddard WA, Skiff WM (1992) UFF, a full periodic table force field for molecular mechanics and molecular dynamics simulations. *J Am Chem Soc* 114:10024–10035.
58. VandeVondele J, et al. (2005) QUICKSTEP: Fast and accurate density functional calculations using a mixed Gaussian and plane waves approach. *Comput Phys Commun* 167:103–128.
59. Hutter J, Iannuzzi M, Schiffmann F, VandeVondele J (2014) CP2K: Atomistic simulations of condensed matter systems. *Wires Comput Mol Sci* 4:15–25.
60. Perdew JP, Burke K, Ernzerhof M (1996) Generalized gradient approximation made simple. *Phys Rev Lett* 77:3865–3868.
61. Grimme S, Ehrlich S, Goerigk L (2011) Effect of the damping function in dispersion corrected density functional theory. *J Comput Chem* 32:1456–1465.
62. VandeVondele J, Hutter J (2007) Gaussian basis sets for accurate calculations on molecular systems in gas and condensed phases. *J Chem Phys* 127:114105.
63. Goedecker S, Teter M, Hutter J (1996) Separable dual-space Gaussian pseudopotentials. *Phys Rev B* 54:1703–1710.
64. Krack M (2005) Pseudopotentials for H to Kr optimized for gradient-corrected exchange-correlation functionals. *Theor Chem Acc* 114:145–152.
65. Plimpton S (1995) Fast parallel algorithms for short-range molecular dynamics. *J Comput Phys* 117:1–19.
66. Blatov VA, Shevchenko AP, Proserpio DM (2014) Applied topological analysis of crystal structures with the program package ToposPro. *Cryst Growth Des* 14:3576–3586.
67. Blatov VA, Delgado-Friedrichs O, O'Keeffe M, Proserpio DM (2007) Three-periodic nets and tilings: Natural tilings for nets. *Acta Crystallogr Sect A* A63:418–425.
68. Ramsden SJ, Robins V, Hyde ST (2009) Three-dimensional Euclidean nets from two-dimensional hyperbolic tilings: Kaleidoscopic examples. *Acta Crystallogr Sect A* A65:81–108.
69. Alexandrov EV, Blatov VA, Kochetkov AV, Proserpio DM (2011) Underlying nets in three-periodic coordination polymers: Topology, taxonomy and prediction from a computer-aided analysis of the Cambridge structural database. *CrystEngComm* 13:3947–3958.
70. Macrae CF, et al. (2006) Mercury: Visualization and analysis of crystal structures. *J Appl Crystallogr* 39:453–457.
71. Brakke KA (1992) The surface evolver. *Exper Math* 1:141–165.
72. Brakke KA, Triply periodic minimal surfaces. Available at facstaff.susqu.edu/brakke/evolver/examples/periodic/periodic.html. Accessed October 3, 2017.